

Fractals in Nature

Vaishnav V. Rao¹, Harshda Saxena¹, B. Malavika¹, Manan Seth¹

Abstract—The laws that govern the creation of fractals seem to be found throughout the natural world. From cosmology to bacterial cultures, self-similarity and fractal geometry is observed in numerous natural objects. Fractals seem to be the preferred design principle for maximizing efficiency in nature. In this report we simulate some famous fractals like the Mandelbrot set and the Koch curve using Python, and study fractal formation in snowflakes, bacterial cultures, ferns and broccoli in detail. This entails an analysis of the results of experiments and computational simulations borrowed from various research papers.

Index Terms—fractals, nature, snowflakes, bacteria

A. Computational approach to Fractals

1) *Mandelbrot and Julia set*: The Mandelbrot set in the complex plane is the set of values of c for which the complex polynomial

$$z_{n+1} = z_n^2 + c \quad (1)$$

remains bounded when iterated from $z_0 = 0$. The filled Julia-set for Eq. 1 is the collection of all the values z_0 for which the polynomial does not diverge.

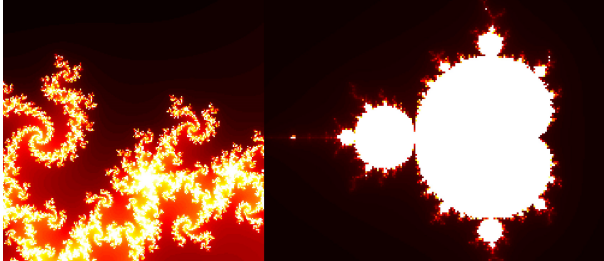


Fig. 1: The Julia set and the Mandelbrot set. The code to the plots are in our [GitHub repository](#).

2) *L-system*: A Lindenmayer system, also known as an L-system, is a string rewriting system, and a type of formal grammar, that due to the recursive nature of the algorithm, can be used to generate fractals with dimension between 1 and 2. It is defined as a tuple, $G = (V, \omega, P)$, where V is a set of symbols containing variables and constants, ω is the initiator, defining the initial state of the system and P is a set of production rules or productions defining the way variables can be replaced with combinations of constants and other variables. The rules of the L-system grammar are applied iteratively starting from the initial state. The cantor set can be drawn as, with A as draw forward, and B as move forward:

```
variables = A, B
constants = none
start = A
rules = (A → ABA), (B → BBB)
```

3) *Koch curve*: In the L-system, an order 4 Koch snowflake is represented as

```
axiom = F --F --F
rules = F → F + F --F + F
iterations = 4
angle = 60°
```

where ' F ' is forward, '+' is anticlockwise rotation by given angle, '-' is clockwise rotation by given angle and axiom is the starting geometric figure (triangle). Now, implementing this through a Python code gives Figure 2.

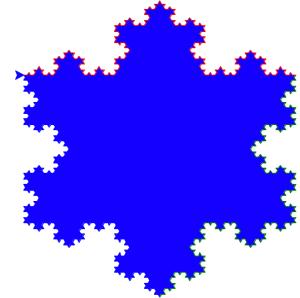


Fig. 2: Numerically generated Koch Snowflake (4 iterations).

I. SNOWFLAKES

Snowflake formation requires subtle physics that to this day is not well understood. Complex shapes emerge as these crystals move through differing temperature and humidity regimes, so that individual snowflakes are nearly unique in structure. An intuitive explanation to the fractal geometry exhibited by snowflakes follows from the fact that no two snowflakes are formed in the exact same way, and that they are sensitive to changes in environmental conditions. A description of a finer theoretical continuum model is found in our [GitHub repository](#).

A. A simple Model

To avoid complications arising just below 0°C due to melting, and other factors, we focus on temperatures between -10°C and -20°C . Three main effects govern the development of snowflakes -

- Diffusion-limited solidification - Depletion of vapor upon growth makes protrusions more accessible and promotes irregular growth and branching.
- Anisotropic attachment kinetics - Molecules have more difficulty bonding to a relatively flat portion of the boundary than to a rougher concave part. This effect tends to regularize shape.

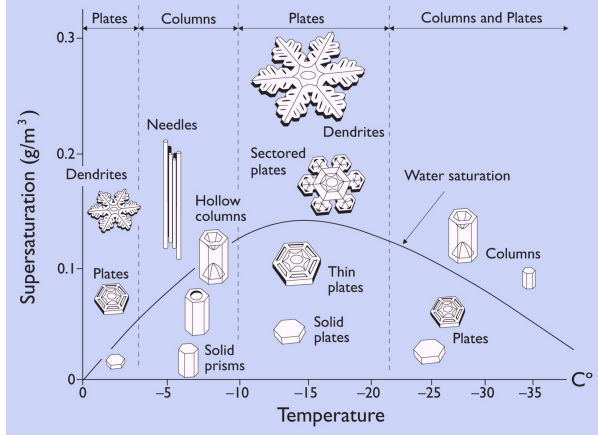


Fig. 3: Nakaya Diagram - Structural dependence of snowflakes on temperature and supersaturation [1].

- Quasi-liquid layer - Very near the crystal surface, these molecules are bound more tightly than in the surrounding vapor, but not completely constrained to the lattice.

The model we will now present for ideal planar snowflake dynamics makes assumptions to study a planar hexagonal prism with major growth on the edges, neglecting melting and others factors. In this model, each site is a cell having 6 neighbours, on our triangular lattice \mathcal{T} . At each discrete time t , and with each site $x \in \mathcal{T}$ we associate a Boolean variable and three varieties of mass. Formally, the state of the system at time t at site x is $\xi_t(x) = (a_t(x), b_t(x), c_t(x), d_t(x))$ where $a_t(x) = 1$ if x belongs to the crystal at time t , and 0 otherwise. $b_t(x)$ is the boundary mass at x at time t (quasi-liquid), $c_t(x)$ is the crystal mass at x at time t (ice), and $d_t(x)$ is the diffusive mass at x at time t (vapor).

B. Numerical algorithm

For the above model, we initialize a mesoscopic prism at the origin surrounded by homogeneous vapor with density ρ , $a_0 = c_0 = 1, b_0 = d_0 = 0$ and for all $x \neq 0$, $a_0(x) = b_0(x) = c_0(x)$ and $d_0(x) = \rho$. We define the notation used as follows -

$$\mathcal{N}_x = \{x\} \cup \{y : y \text{ is a nearest neighbor of } x \text{ in } \mathcal{T}\}$$

$$A_t = \{x : a_t(x) = 1\} = \text{the snowflake at time } t$$

$$\partial A_t = \{x \notin A_t : a_t(y) = 1\} \text{ for some}$$

$$y \in \mathcal{N}_x = \text{the boundary of the snowflake at time } t$$

$$A_t^c = \{x : a_t(x) = 0\} = \text{the sites not in } A_t$$

$$\bar{A}_t^c = (A_t \cup \partial A_t)^c = \text{the sites not in } A_t \text{ or } \partial A_t$$

\circ denotes amount of mass before and $'$ denotes after a discrete iteration.

The first step is to model diffusion. Diffusive mass evolves on the crystal by discrete diffusion with uniform weight 1/7 on the center site and each of its neighbors, that is -

$$d'_t(x) = \frac{1}{7} \sum_{y \in \mathcal{N}_x} d_t^o(y) \quad \text{for } x \in \bar{A}_t^o \quad (2)$$

whereas for $x \in \partial A_t$ any term in the sum of $y \in A_t$ is replaced by $d_t^o(x)$.

The second step is to model Freezing. κ models the proportion of diffusive mass crystallizing at boundaries, that is for $x \in \partial A_t$ -

$$b'_t(x) = b_t^o(x) + (1 - \kappa)d_t^o(x) \quad (3)$$

$$c'_t(x) = c_t^o(x) + \kappa d_t^o(x) \quad (4)$$

$$d'_t(x) = 0 \quad (5)$$

To model attachment, we decide when a boundary site joins the snowflake, these depend on $n_t^o(x) = \text{no of } \{y \in \mathcal{N}_x : a_t^o(y) = 1\}$ as with parameters θ, β, α for $x \in \partial A_t^o$ -

$$\text{If } n_t^o = 1 \text{ or } 2 \text{ and } b_t^o(x) \geq \beta \quad (6)$$

$$\text{If } n_t^o = 3 \text{ } b_t^o(x) \geq 1 \text{ or } (\sum_{y \in \mathcal{N}_x} d_t^o(y) \leq \theta \text{ and } b_t^o(x) \geq \alpha) \quad (7)$$

$$\text{If } n_t^o \geq 4 \quad (8)$$

then $a'_t(x) = 1$, $c'_t(x) = b_t^o(x) + c_t^o(x)$ and $b_t^o(x) = 0$.

We finally model melting, as proportion μ of the boundary mass and proportion λ of the crystal mass at each boundary site becomes diffusive mass. That is, for $x \in \partial A_t$ -

$$b'_t(x) = (1 - \mu)b_t^o(x) \quad (9)$$

$$c'_t(x) = (1 - \lambda)c_t^o(x) \quad (10)$$

$$d'_t(x) = d_t^o(x) + \mu b_t^o(x) + \lambda c_t^o(x) \quad (11)$$

C. Results

In this section, we see the roles that each parameter has on the geometry, and growth of snowflakes, from simulations run by the authors in [2]. The role of vapor density or ρ , is

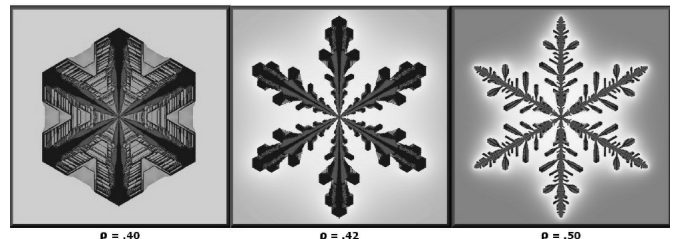


Fig. 4: Dependence of Morphology on ρ [2].

closely related to supersaturation and the crystals grow more rapidly as ρ increases; and transition in morphology from plate to sectored plate to dendrite. The plate case exhibits delayed, thin filling of concavities due to the knife-edge instability (on making the edge a bit thinner, attachment kinetics dictates that the intrinsic growth rate of the edge will increase, causing it to sharpen, and a positive feedback that enhances the crystal growth and drives the formation of thin, platelike structures)

The additional increase of β from 1 controls the anisotropy of attachment. Higher anisotropy promotes faceting and a transition from fern to dendrite to sectored plate. Increasing β delays the onset of the first instability, increasing the size of the central hexagonal plate before main branches develop. It also diminishes the propensity for side branching.

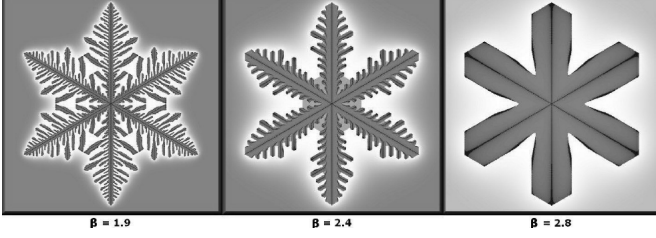


Fig. 5: Dependence on β [2].

The dependence on α and θ is still speculative. Tuning them controls both the strength and the geometry of the implementation. The closer θ is to 0, the more delay there is in attachment off the ridges. The closer α is to 0, the more the instability manifests itself in concavities between ridges rather than along sides of ridges, and this offers the only explanation for faceted growth after depletion of vapour.

According to the freezing step, κ proportion of vapour

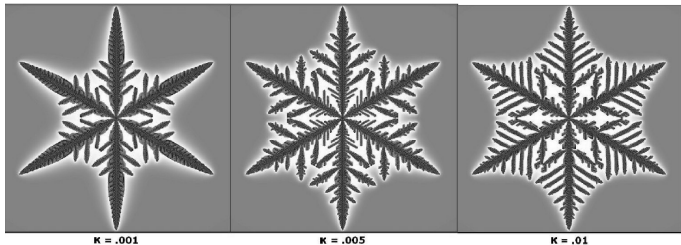


Fig. 6: Dependence on κ [2].

is deposited directly as ice and simply waits to attach to the snowflake. Such ice does not enter into the attachment step. Since vapor is most concentrated near tips of the main branches, increasing κ tends to deprive these tips of more boundary mass than the tips of side branches. Consequently, simulations with very small κ have less side branching than those with a somewhat larger value.

The melting step has an effect opposite to that of freezing

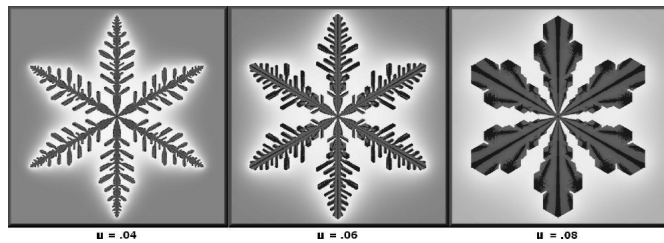


Fig. 7: Dependence on μ [2].

and increasing μ promotes faceting. The role of λ is very similar but will typically be much smaller. As melting increases further, though, hexagonal tips become evident first on the main branches, then on the larger and less frequent side branches, changing from a stellar dendrite to a stellar plate.

In this whole analysis however, we have neglected the role of velocity, which can be incorporated by adding a continuous boost in supersaturation, and a sudden decrease in ρ when the crystal leaves the cloud cover, and in this process, κ

also changes. These can be incorporated in the simulations, and after adding some noise, create very realistic snowflakes. The real problem is much more complicated however, and future research areas include a detailed analysis of the phase portrait, incorporating sublimation, developing 3-D models, among others.

II. FRACTALS IN BACTERIAL COLONIES

While tracking the development of fluorescence labeled cellular domains in surface growing *E. coli*, the emergence of striking fractal patterns with jagged, self-similar shapes was observed. In this section we try to look at some of the underlying causes of such global self-similarity by understanding the results of experiments and computer simulations run by T. J. Rudge et al., 2013 [3]. We then briefly look at how fractal dimension is calculated in bacterial populations.

A. The Experiment

Two isogenic populations of *E. coli* were marked by transforming them with plasmids expressing different fluorescent proteins. Agar plates were then seeded with equal densities of cells of each type, such that distinct domains formed from spatially separated single cells. These domains grew to be adjacent, enabling examination of their physical interactions. The boundaries between these domains were punctuated by repeated angular folds, giving a self-similar fractal appearance observable at many scales from micrometers to millimeters. The fractal dimension of the boundaries of multiple domains was calculated to be 1.23 ± 0.041 .

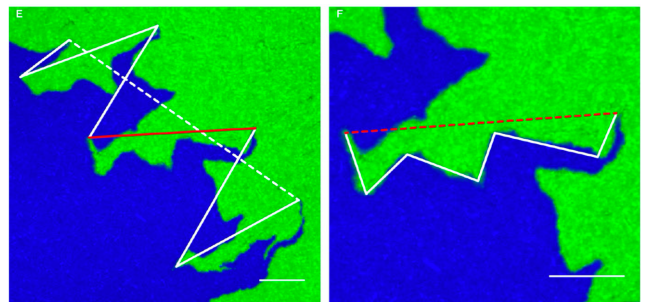


Fig. 8: Self-similar boundary between two populations of cells. The red solid line in the left image represents a smaller boundary analyzed at a lower scale in the left image. Scale bars 30 μm [3].

B. The Model

E. coli is a rod-shaped bacterium, roughly cylindrical with hemispherical ends, forming a capsule that exhibits extremely regular growth and division dynamics. Thus, to simulate this phenomenon, a model was created on CellModeller under the assumptions that cells are rigid, elongating, nonmotile capsules that divide exactly in half. Further, it was assumed that the growth rate is proportional to length and growth is constrained by forces between cells and viscous drag. The computational simulation of such a model resulted in emergent self-similar fractal patterns that had striking resemblance with the patterns observed experimentally. Moreover,

the fractal dimensions of these simulations calculated for different initial conditions was found to be consistent with the fractal dimension observed through confocal microscopy of *E. coli* populations.

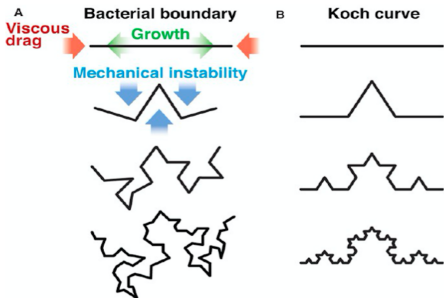


Fig. 9: (A) Schematic representation of fractal boundary emergence in bacterial populations. (B) Mathematical generation of the Koch curve. Observed value of fractal dimension for *E. coli* domain boundaries match with the dimension of the Koch curve which is $\ln 4/\ln 3 \approx 1.26$ [3].

C. Physical explanation

The model described above generates lines or files of cells due to the axial alignment of growth and division. It also generates compressive forces (which increase as file size increases) due to the opposition of viscous drag to cell growth. Slight perturbations in the daughter cell orientations, which physically correspond to imperfections in cell shape or Brownian motion, create local asymmetries. It is expected that these local asymmetries become unstable above some critical level of compressive force, leading to buckling of cell files (Fig. 9). Further cell growth and division will cause the new files to expand and should cause this process to repeat each time the local compressive forces become large enough, resulting in self-similar patterns of angular folds.

D. Factors affecting fractal dimension

Our analysis in the previous section suggests that the degree of cell polarity (spatial anisotropy of a cell) should impact the extent to which a domain boundary ‘folds’. To confirm this hypothesis, the model was tweaked by giving cell capsules different aspect ratios. Keeping the diameter of the capsule constant it was found that the calculated fractal dimension reduced as length decreased. Moreover, simulations showed that self similarity disappeared for spherical cells. This interesting result was confirmed *in vivo* through mutant *E. coli* populations that produced spherical cells. Further, minimizing other parameters such as growth rate and division rate on CellModeller also resulted in smoother boundaries and smaller fractal dimensions.

E. Calculation of Fractal Dimension

Apart from exhibiting self-similarity at domain boundaries, bacterial colonies themselves tend to exhibit fractal nature as a whole (Figure 10). We now take a look at a method of calculating the fractal dimension for such a bacterial colony.

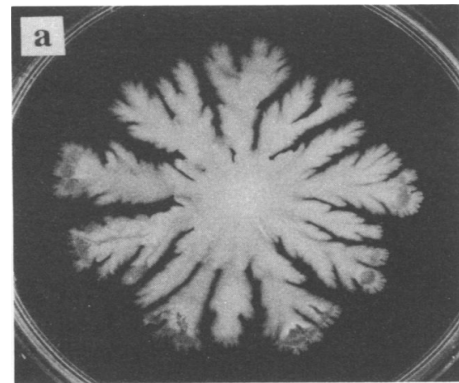


Fig. 10: Fractal nature of a *K. pneumoniae* giant colony [4].

This procedure employs a method of “pixel counting” which is exactly how the box dimension is calculated [4].

The overall colony size is calculated by determining the radius of gyration (R_G)

$$R_G^2 = \frac{1}{N} \sum_{i=1}^N (\mathbf{r}_i - \mathbf{r}_c)^2 \quad (12)$$

where N is the number of pixels occupied by the pattern, \mathbf{r}_i is the position vector of the i th occupied pixel, and \mathbf{r}_c is the position vector of the center of mass for all occupied pixels:

$$\mathbf{r}_c = \frac{1}{N} \sum_{i=1}^N \mathbf{r}_i \quad (13)$$

If the pattern is self-similar and the values of N and R_G at several stages of the growing pattern are able to be evaluated, there exists a simple relation:

$$N \sim R_G^{D_f} \quad (14)$$

where D_f is the fractal dimension of the pattern. Now, R_G is inversely proportional to the pixel size, p , because length is scaled as p^{-1} . Using this relation, the number of occupied pixels of size p is scaled as

$$N(p) \sim p^{-D_f} \quad (15)$$

Now, the fractal dimension of the bacterial colony can be calculated by plotting the log-log graph of the datum points (N, p) and taking the negative value of the slope.

F. Significance

The engineering of patterning and fate in cell populations remains a major goal of synthetic biology. Potential applications range from artificial organization of biofilms for enhanced catalysis, to the engineering of artificial tissues and organs in multicellular organisms. There are a wide range of potential benefits that would arise from the ability to engineer the flow of metabolites through specialized cell populations and storage of products in harvestable form.

III. FRACTALS IN FERNS

Ferns are an ancient group of green flowerless plants that have divided leaves known as fronds. The fractal-like nature displayed by fronds of ferns is perhaps one of the most famous examples of self-similarity observed in nature.

A. Structure of a frond

An entire fern is mostly built up from the same basic shape repeated over and over again at ever smaller scales. Ferns are pinnate, which means they have leaflets (pinnae) arranged on either side of the stem (petiole). In some fronds the pinnae are further divided into segments called pinnules. The fronds can be classified on the basis of the degree of division of the pinnae. Thus a fern which is a bipinnate pinnatifid (for instance

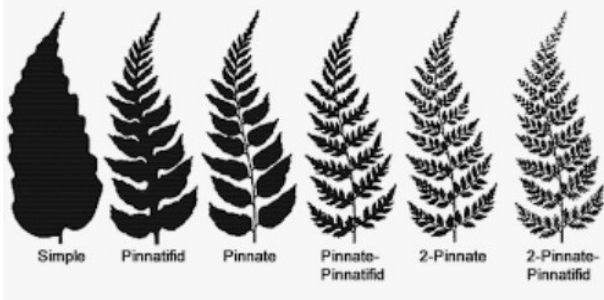


Fig. 11: Classification of fern fronds by their pinnate structure [5].

the *Dryopteris expansa*) has two levels of self similarity, that is, the pinnae are divided in a way such that the pinnules have a structure that is similar to the shape of the original frond. Thus ferns have an approximate fractal nature because they have a finite degree of pinnation. A fern with infinite self-similarity is a fractal and we will describe such a fern in the next section.

B. Barnsley's Fern

Barnsley's Fern is a fractal named after the British Mathematician, who first described it in his book *Fractals Everywhere* [6]. It is made to resemble the *Asplenium adiantum-nigrum* (black spleenwort) variety of fern. Barnsley's Fern is created by iterating over a large number of times on four mathematical equations, introduced by Barnsley, known as Iterated Function System (IFS). The attractor of the IFS is given by a set of four affine transformations [6]

$$f_1(x, y) = \begin{bmatrix} 0.85 & 0.04 \\ -0.04 & 0.85 \end{bmatrix} \begin{bmatrix} x \\ y \end{bmatrix} + \begin{bmatrix} 0.00 \\ 1.60 \end{bmatrix} \quad (16)$$

$$f_2(x, y) = \begin{bmatrix} -0.15 & 0.28 \\ 0.26 & 0.24 \end{bmatrix} \begin{bmatrix} x \\ y \end{bmatrix} + \begin{bmatrix} 0.00 \\ 0.44 \end{bmatrix} \quad (17)$$

$$f_3(x, y) = \begin{bmatrix} 0.20 & -0.26 \\ 0.23 & 0.22 \end{bmatrix} \begin{bmatrix} x \\ y \end{bmatrix} + \begin{bmatrix} 0.00 \\ 0.44 \end{bmatrix} \quad (18)$$

$$f_4(x, y) = \begin{bmatrix} 0.00 & 0.00 \\ 0.00 & 0.16 \end{bmatrix} \begin{bmatrix} x \\ y \end{bmatrix} \quad (19)$$

with probability factors $p_1 = 0.85, p_2 = 0.07, p_3 = 0.07, p_4 = 0.01$, thereby generating the successively smaller leaflets, the largest right-hand leaflet, the largest left-hand leaflet and the stem respectively. Implementing this through a Python code gives the final output in Fig. 12.

IV. FRACTALS IN BROCCOLI

One of the most visually appealing examples of fractals in plants is the Romanesco broccoli. This alien-looking, nutty flavoured broccoli is a striking example of how simple natural evolution can produce such complex patterns.

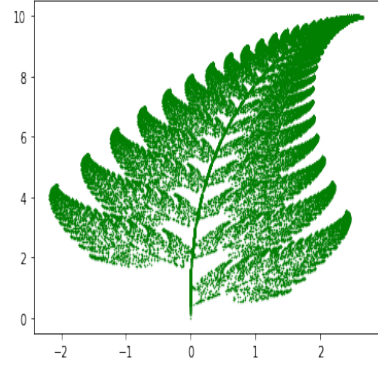


Fig. 12: Barnsley's Fern plot.

A. Structure of Broccoli

The vertical cross section of a regular variety green broccoli has been mapped to a Pythagoras tree [7]. This is a kind of fractal which is constructed iteratively over squares. To one side of a square, a right angled triangle is added whose smaller sides are extended to form squares of the next iteration. This process is repeated exactly to form a tree. Direct scanning of the cross sections has been employed to calculate the fractal dimension using the box dimension definition. For a three dimensional object, part of the method used in subsection II-E can be simply extended. Since it is much easier to observe fractals embedded in one or two dimensions and the dimensions of cross section of fractals are related to those in the bulk, the method of “pixel counting” can be employed. If the dimension of a fractal embedded in a cross section is D_c and that of the bulk is D , the relation

$$D = \frac{3}{2N} \sum_{i=1}^N D_{c_i} \quad (20)$$

is used in the case of i cross sections.

From this method, the D_c of 1.78 ± 0.02 was obtained [8]. Since the different directions were independent, the final capacity dimension was determined to be 2.7. This dimension was then used to find the parameters of a symmetric Pythagoras tree which would match the dimension. The fractal dimension of a Pythagoras tree is given by

$$D_c^{(t)} = \frac{\log 2}{-\log t} \quad (21)$$

where t is the scale factor to be determined. From the cross sectional dimension, $t = 0.68$ was obtained, which was used to calculate the angle of the right isosceles triangle using the relation

$$t = \frac{1}{2 \cos \theta} \quad (22)$$

giving $\theta \approx 43^\circ$. Thus the Pythagoras tree of Fig. 13 was generated.

B. Romanesco and Logarithmic Spirals

The fractal structure present in Romanesco is quite different to the Green Broccoli discussed earlier. This appears to follow a logarithmic spiral pattern as seen in Fig. 14.

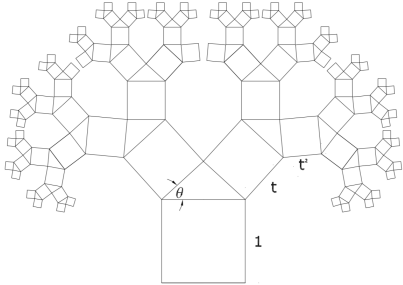


Fig. 13: Pythagoras Tree modelling Green Broccoli [8].

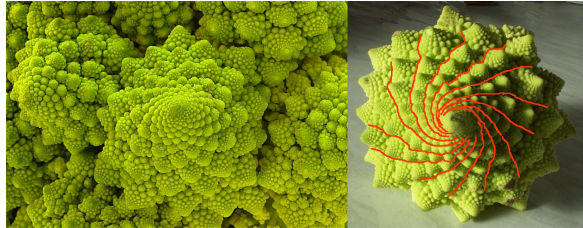


Fig. 14: The left image is a close up of Romanesco broccoli [9]. The right image roughly traces out logarithmic spirals on it [10].

A logarithmic spiral is defined in polar coordinates by the equation

$$\varphi = \frac{1}{k} \log \left(\frac{r}{a} \right) \quad (23)$$

This is a self similar fractal as rotating this curve by φ_0 is equivalent to scaling it by a factor of $e^{-k\varphi_0}$. Thus scaling the curve by a factor of $e^{k*2n\pi}$ gives us back the same curve which explains their fractal nature.

REFERENCES

- [1] John Barrett, Harald Garcke, and Robert Nürnberg, “Numerical computations of faceted pattern formation in snow crystal growth,” *Physical Review E*, Vol. 86, 02 2012.
- [2] Janko Gravner and David Griffeath, “Modeling snow crystal growth II: A mesoscopic lattice map with plausible dynamics,” *Physica D: Nonlinear Phenomena*, Vol. 237, pp. 385–404, 03 2008.
- [3] Timothy J. Rudge, Fernán Federici, Paul J. Steiner, Anton Kan, and Jim Haseloff, “Cell Polarity-Driven Instability Generates Self-Organized, Fractal Patterning of Cell Layers,” *ACS Synthetic Biology*, Vol. 2, No. 12, pp. 705–714, 2013, PMID: 23688051.
- [4] T Matsuyama and M Matsushita, “Self-similar colony morphogenesis by gram-negative rods as the experimental model of fractal growth by a cell population.,” *Applied and Environmental Microbiology*, Vol. 58, No. 4, pp. 1227–1232, 1992.
- [5] U.S. Forest Service, <https://www.fs.fed.us/wildflowers/beauty/ferns/structure.shtml>.
- [6] Michael F Barnsley, *Fractals everywhere*, Academic press, 2014.
- [7] Heinz-Otto Peitgen, Hartmut Jürgens, and Dietmar Saupe, *Chaos and fractals: new frontiers of science*, Springer Science & Business Media, 2006.
- [8] Sang-Hoon Kim, “Fractal dimensions of a green broccoli and a white cauliflower,” *arXiv preprint cond-mat/0411597*, 2004.
- [9] John Walker, “Fractal food: Self-similarity on the supermarket shelf,” *Fractal Food*, 2005.
- [10] “Fibonacci Numbers and Nature,” <http://www.maths.surrey.ac.uk/hosted-sites/R.Knott/Fibonacci/fibnat.html#veg>, Accessed: 2020-12-06.
- [11] Steven H. Strogatz, *Nonlinear Dynamics and Chaos: With Applications to Physics, Biology, Chemistry and Engineering*, Westview Press, 2000.